Article:
Li, P., Susmel, L. and Ma, M. (2023) The life prediction of notched aluminum alloy specimens after laser shock peening by TCD. International Journal of Fatigue, 176. 107795. ISSN: 0142-1123

https://doi.org/10.1016/j.ijfatigue.2023.107795

The life prediction of notched aluminum alloy specimens after laser shock peening by TCD

Piao Li [a] Luca Susmel [a] Mingze Ma [b*]

(a Department of Civil and Structural Engineering, The University of Sheffield, Sheffield S1 3JD, UK)

(b College of Aerospace Engineering, Nanjing University of Aeronautics and Astronautics, Nanjing 210016, China)

Abstract: The effect of Laser shock peening (LSP) on the fatigue life of notched metallic specimens is studied. LSP is applied to notched specimens made of two aluminum alloys and the fatigue tests are carried out. The stress field at the notch is both measured by X-ray diffractometer and simulated through numerical methods. The highest compressive stress lies in the layer near but a little below the surface. A life prediction method is proposed by introducing the effective stress after LSP into the Theory of Critical Distances (TCD). The predicted results are in sound agreement with the test results.

Keywords: Aluminum alloy, Notched specimen, TCD, Fatigue life, Laser shock peening (LSP)

1 Introduction

Laser shock peening (LSP) is a surface strengthening technology that uses high-strength compressive stress shock wave generated by high-energy pulsed laser beam to induce surface deformation on metallic materials. Nowadays this technology is commonly used in the field of aeronautics as an anti-fatigue design method. After using laser beam, a certain level of residual compressive stress remains in the surface layer of the impacted area. Mironov et al. [1] studied the

* Corresponding author. E-mail address: mamingze@nuaa.edu.cn

relationship between the residual stress and the microstructure evolution during LSP, and came to the conclusion that the unique residual-stress state generated during LSP is associated with the very high imposed energy and the short time scale of the process. The generated residual compressive stress is beneficial to reduce the level of tensile stress when alternating load is applied. The existence of compressive stresses, on one side, weakens the average stress and, on the other side, favors the crack closure effect. Accordingly, it can be an effective way to improve the fatigue performance of metallic materials. However, the fatigue life analysis of the structure after LSP is complex and remains an important but difficult problem.

Some research work has already been conducted on the LSP-related fatigue behavior of materials or structures, among which the effect of LSP parameters on fatigue performance has been extensively studied. Jiang et al. [2] investigated the effect of laser power density on the fatigue life and fracture characteristics of 7050-T7451 aluminum alloy specimens with fastener holes. Spadaro et al. [3] studied the influence of LSP with different pulse densities on the low cyclic fatigue behavior of superferritic stainless steel UNS S 44600. Yella et al. [4] investigated the influence of LSP on the fatigue behavior of 316LN stainless steel and demonstrated that the fatigue life is dependent on the material surface condition and the employed stress amplitude. Prabhakaran et al. [5] completed the fatigue test of a high strength ultrafine bainitic steel with and without LSP. They showed that, on average, the high-cycle fatigue life of those specimens treated with LSP was about five times longer than that of the untreated specimen. Zhang et al. [6] investigated the fatigue behavior of a medium carbon steel with LSP and shot peening (SP). Dwivedi et al. [7] investigated the effect of LSP on the surface properties and ratcheting behavior of a high strength low alloy steel. The results showed that LSP improved the surface mechanical properties significantly. Azevedo et

al. [8] presented experimentally the fatigue behavior of AISI D2 tool steel samples subjected to LSP with a power density of 15 GW/cm^2. It was shown that the fatigue strength of LSP-treated samples was 32.9% higher compared to that of untreated samples due to the existence of significant compressive residual stresses in a superficial layer of the material. Lu et al. [9], Bikdeloo et al. [10] and Li et al. [11] investigated the effect of multiple LSP. In parallel, Correa et al. [12], Adu-Gyamfi et al. [13], Larson et al. [14] and Aswegen et al. [15] investigated the effect of the scanning pattern of LSP and it was shown that the pattern of scanning affects residual stress distribution.

LSP causes residual stress on the surface of the specimen and the surface properties have a significant influence on the fatigue properties of the material. Luo et al. [16] and Wei et al. [17] simulated the LSP residual stress in the depth direction from the specimen surface using finite element methods (FEM) and compared the simulated results with experimental data. Salimianrizi et al. [18] and Keller et al. [19] conducted experimental and numerical investigation of residual stresses under different laser power densities and scanning patterns. Gao et al. [20] investigated the effect of residual stress distribution caused by LSP on the HCF properties of a nickel aluminium bronze (NAB) alloy, and it is indicated that the HCF life under different laser pulse energies can be predicted by using the fatigue stress concentration factor. Sanchez et al. [21] proposed that LSP generated deep compressive residual stress at a level of above -300 MPa, and the overall fatigue life increased by two-order magnitude.

The hole, pin or bolt connection are typical structural discontinuities of engineering components, and the application of LSP technology to these discontinuous components has also been studied by different researchers. Cuellar et al. [22] investigated the residual stress distribution in the vicinity of the hole under various laser shock peening patterns. Ivetic et al. [23] investigated

the effects of the sequence of open-hole drilling on the fatigue life. This study indicated that a negative effect was encountered on the open-hole thin aluminum specimens without LSP treatment, while positive effect was observed in specimens in which the hole was drilled after LSP treatment. Sun et al. [24] carried out LSP treatment to some 2024-T351 aluminum alloy specimens with circular holes then conducted high cycle fatigue tests on these specimens. The results showed that the fatigue life of LSP treated specimens extended by 2 to 3 times due to a compressive residual stress layer introduced by LSP. The above studies were conducted to study the effect of LSP on the fatigue properties of metallic notched components, however, there is still a lack of reliable life prediction methods that can be used to predict the fatigue life of these LSP-treated notched components. Since the stress concentration at the notch and the treatment of LSP together lead to a more complex stress distribution, the life prediction of such notched components is more difficult. However, due to the effectiveness of LSP in the enhancement of fatigue resistance of notched components in engineering, there is a necessity to develop practical life prediction methods for these components.

There are many approaches proposed for the fatigue life prediction of notched specimens, among which the Theory of Critical Distances (TCD) [25-27] and the Stress Field Intensity (SFI) approach [28] are widely accepted and adopted. Based on these two theory systems, some other methods have also been developed. For example, Susmel [29] connected the critical plane method with the point method in TCD to predict the multiaxial fatigue life of notched components. Shang [30] proposed the stress-strain field intensity method to predict the low-cycle fatigue life of notched specimens. Due to the practicability and rationality of the TCD, it has long been popular in the field of fatigue life analysis. In this paper, the effective stress after LSP is introduced into the TCD to

predict the fatigue life of notched components. It is worth noting that the initial stress before LSP and the compressive stress after LSP are all considered in the effective stress. A complete life prediction procedure is constructed by combining the LSP feature with the TCD, and fatigue tests were carried out on two notched aluminum alloy specimens for verification.

2 Materials and Specimens

2.1 Materials

The materials being tested were 2024-T351 and 7050-T7451 aluminum alloys, which are commonly used in aeronautical engineering. Standard pieces were made from aluminum alloy sheets with a thickness of 5mm, see Fig. 1. Laser shock peening was applied to both sides of the specimen intermediate region. The power density of the laser was 7.96GW/cm^2, and the laser pulse width was 50ns. Static tests were carried out according to the standard HB5143-1996 “Tensile Test of Metallic materials at Room Temperature”. The static test results are listed in Table 1. In Table 1, the values of the fatigue limit at 10^7 cycles with stress ratio R=0.06 and the stress intensity factor (SIF) threshold ΔK_{th} at stress ratio R=0.06 are taken from the literature [31].

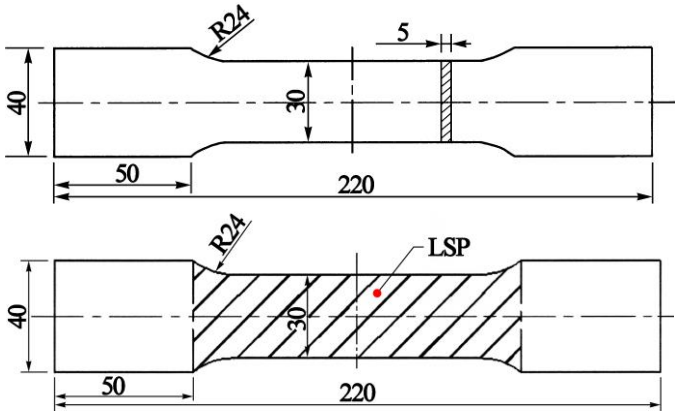

Fig.1. Smooth specimen

Table 1

The mechanical properties of 2024-T351 and 7050-T7451.

Materials		2024-T351		7050-T7451	
		Without LSP	With LSP	Without LSP	With LSP
Yield strength σ_y /MPa	Test value	365.02, 364.56, 361.43, 357.59, 351.86	370.17, 372.76, 368.54, 370.05, 373.23	478.86, 479.90, 472.27, 480.56, 474.71	496.53, 489.62, 502.81, 498.25, 491.70
	Average	360.09	370.95	477.26	495.78
	Standard deviation	5.48	1.98	3.60	5.26
Ultimate strength σ_{ult} /MPa	Test value	477.89, 476.06, 472.5, 469.39, 460.61	489.06, 492.06, 486.5, 488.78, 493.33	534.43, 535.89, 522.17, 541.44, 526.79	544.56, 529.22, 554.72, 549.89, 529.33
	Average	471.29	489.95	532.14	541.54
	Standard deviation	6.81	2.74	7.65	11.76
Young's modulus *E*/GPa	Test value	69.32, 69.04, 68.87, 67.42, 68.77	68.35, 69.56, 67.43, 69.31, 68.54	64.5, 65.27, 63.69, 65.96, 64.37	64.26, 62.85, 64.48, 65.31, 64.86
	Average	68.68	68.64	64.76	64.35
	Standard deviation	0.74	0.84	0.88	0.93
Fatigue limit (R=0.06, 10^7cycles) σ_e /Mpa [31]		220.1	—	190.4	—
SIF threshold ΔK_{th} / $\mathrm{MPa}\sqrt{\mathrm{m}}$ [31]		4.68	—	3.57	—

2.2 Specimens

The notched specimens, as shown in Fig. 2, were made from 2024-T351 and 7050-T7451 aluminum alloy sheets with a thickness of 5mm. The tested specimens with their serial numbers are listed in Table 2.

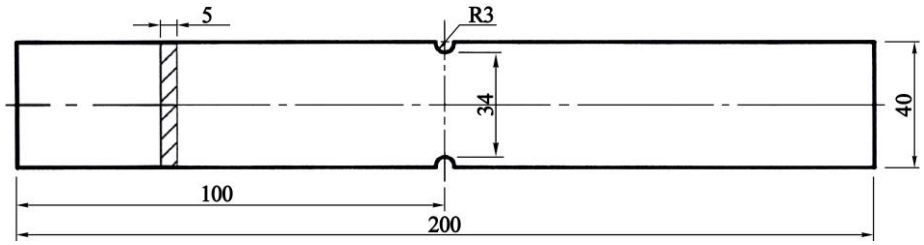

Fig.2. Configuration of notched specimen

Table 2

Notched specimen arrangement.

Specimen material	Status	Quantities	Serial number
2024-T351	Without LSP	10	SY6-1-1 ~ SY6-1-10
	With LSP	10	SY6-3-1 ~ SY6-3-10
7050-T7451	Without LSP	10	SY6-4-1 ~ SY6-4-10
	With LSP	10	SY6-6-1 ~ SY6-6-10

2.3 LSP and residual stress

Before the LSP process was applied, the residual stresses at point A just in front of the notch root (as shown in Fig. 3) of every specimen were measured by using the Bruker-8D-Advanced X-ray diffractometer. X-ray diffraction is a nondestructive testing method which is commonly used in the measurement of residual stress for brittle and nontransparent materials. The measured results are listed in Table 3. The LSP process was applied on an annular surface in the vicinity of the notches, see Fig. 3. The power density of the laser was 7.96GW/cm^2, and the laser pulse width was 50ns. After the LSP process, the residual stresses at point A were measured again, the residual compressive stresses are also listed in Table 3. It is shown that the residual stress before LSP is about 85MPa, and the stress after LSP is -143MPa for 2024-T351 and -105MPa for 7050-T7451.

One aspect that is worth highlighting is that the LSP process can lead to the change of surface

roughness. The roughness test conducted by Salimianrizi et al. on the LSP treated Al 6061-T6 shows that the surface roughness increases compared to the unprocessed surface [18]. Due to the laser shot, local plastic deformation may occur in the form of a dimple on the surface, and the dimples together form the texture affecting the roughness of the surface [18].

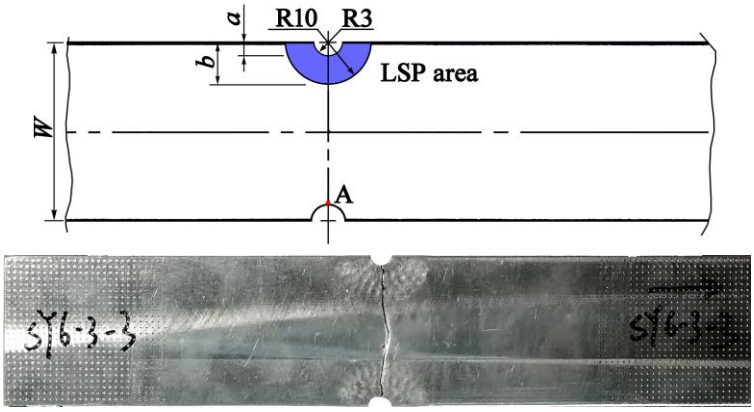

Fig. 3. The LSP area

Table 3

Measured residual stress at point A.

Specimen material	Status	Residual stress σ_r /MPa
2024-T351	Without LSP	85±7
	With LSP	-143±8
7050-T7451	Without LSP	86±9
	With LSP	-105±10

Finite element analysis (FEA) numerical simulations were carried out by using software ABAQUS/Explicit and ABAQUS/Standard [17]. In the numerical model, half of the symmetrical structure of the specimen was modelled and the configuration was exactly the same as the specimen. The laser peening was applied around the notch, and the scanning path of the laser peening was from near to far of the notch root, as shown in Fig. 4.

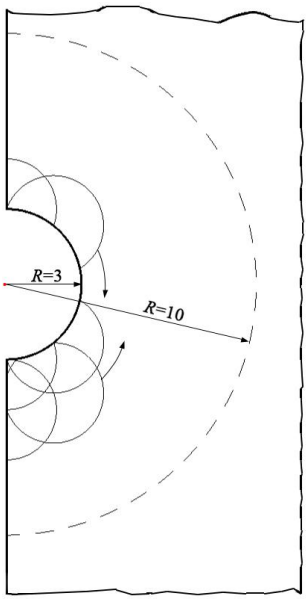

Fig.4. Scanning path of the laser peening

The simulated residual compressive stress distributions are shown in Fig.5. Fig.5(a) presents the residual compressive stress distribution along y direction, which is the thickness direction of the specimen. Fig.5(b) presents the residual compressive stress distribution on the specimen surface along x direction, which is the direction perpendicular to the thickness direction. The surface layer of the specimen is under compressive stress state due to LSP. It can be seen from Fig.5(a) that when it gets deeper in the thickness direction and farther from the surface, the compressive stress increases first and then decreases. It should be mentioned that the actual stress distribution in the specimen should take into account the original measured residual tensile stress (Table 3). Since the residual tensile stress was about 85 MPa at point A of the specimen without LSP, when the residual compressive stress approaches about -85MPa at the thickness of 0.7mm for 2024-T351 specimen and 0.8mm for 7050-T7451 specimen, the combined stress equals zero in the specimen. In other words, the layer thickness of the compressive stress for 2024-T351 specimen is 0.7mm, and that of the 7050-T7451 specimen is 0.8mm. When it gets deeper below the compressive stress layer, the tensile stress appears, and the residual stress curves above the -85MPa show exactly the tensile

stress distributions.

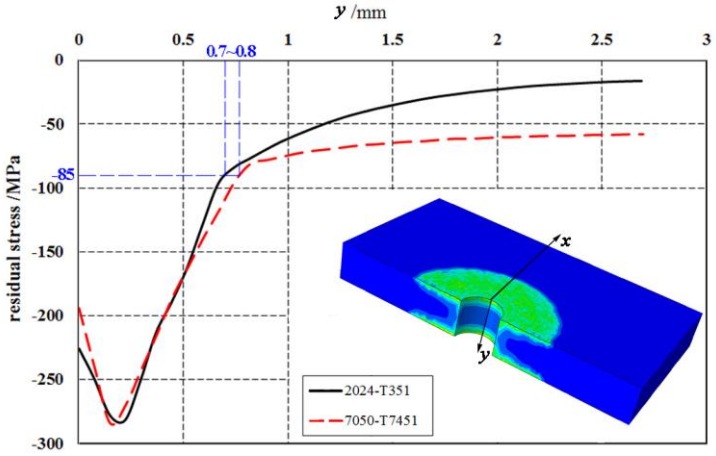

(a) The residual compressive stress distribution along y direction (the thickness direction)

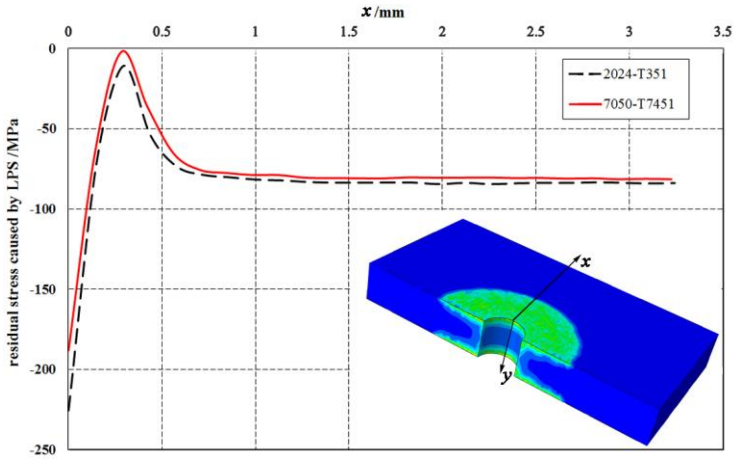

(b) The residual compressive stress distribution on the specimen surface along x direction

Fig.5. The residual compressive stress distribution

2.4 Fatigue test results

The fatigue tests were conducted on a MTS 370.10 test machine. Before fatigue testing, one to four specimens were used for quasi-static tension tests to estimate the ultimate strength of the specimens themselves. Then, based on the S-N curves of the materials and the fatigue notch factors (K_f) of the specimens, the fatigue loading was determined according to the estimation that the fatigue lives of all specimens fell within 10^5 to 3×10^5 cycles. The stress ratio R was 0.06. The fatigue test

results are listed in Table 4, the specimens after tests are shown in Fig. 6.

In the implementation of experiment, the fatigue life is defined as the cycles at which the crack reaches 1mm. The crack propagation length was recorded at different moments by a video camera in the high-speed continuous shooting way. The reason to adopt 1mm as the fatigue life lies in that it is a common method to determine fatigue life in the engineering field. In 1977, Duggan et al. has given a more clear meaning to the fatigue life, defining the life of the actual component before a specified "engineering crack" as crack initiation life [32]. In practice, it is common to take macroscopically visible or detectable cracks as engineering cracks. No strict regulations have been made on the actual size of the “engineering crack”, and in engineering practice, this size is generally taken as 1mm.

Table 4

Fatigue test results (R=0.06).

Materials	Status	S_{max}/MPa	Cycles to crack length 1 mm, N_f	Logarithmic life	
				Average	Standard deviation
2024	Without LSP	106.3	204925，164860，185271，87132，111010 125098，216886，181825，170000	5.1895	0.13294
	LSP	144.5	200024，209643，426256，235129， 253534	5.3748	0.12512
			229919，171648		
7050	Without LSP	85.0	266959，155273，419945，220084， 190907 230273	5.3711	0.14701
	LSP	119.0	322334，176844，330350，221654,231925 314727，314897	5.4260	0.10629

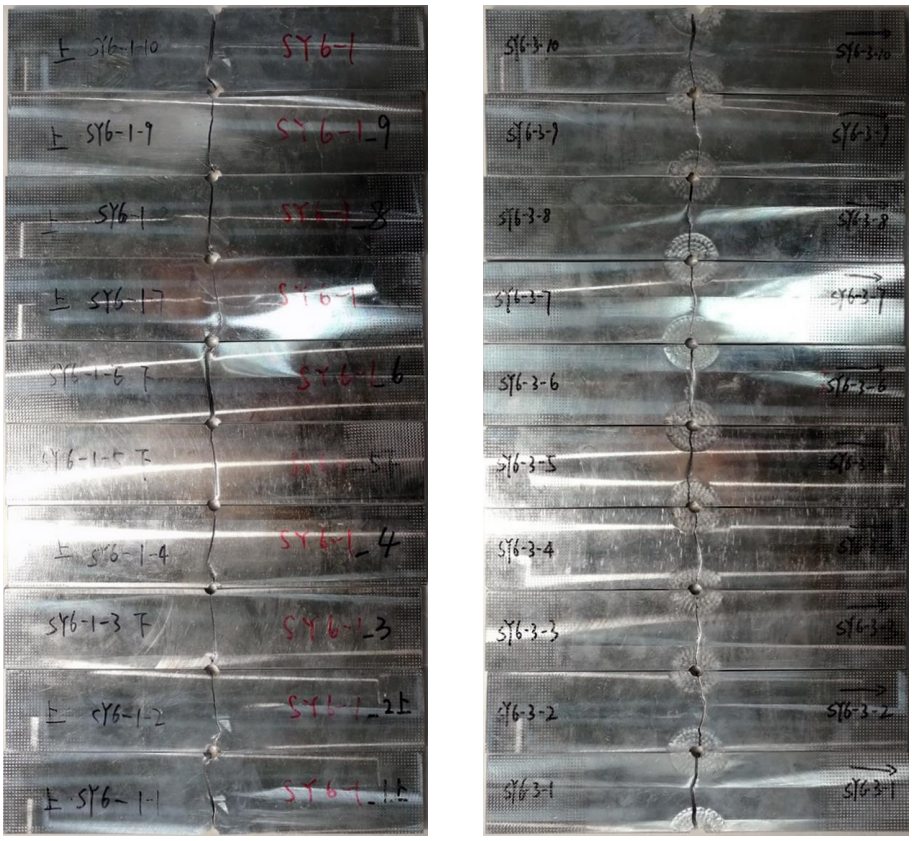

(a) 2024-T351 Specimens without and with LSP

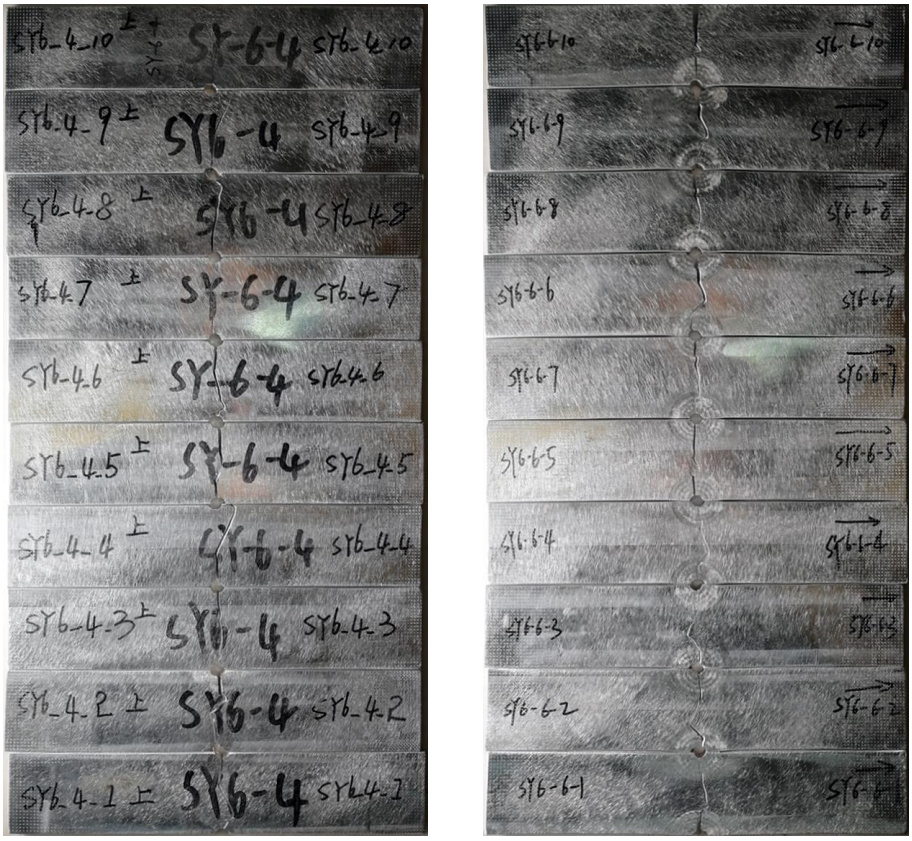

(b) 7050-T7351 specimens without and with LSP

Fig. 6. Specimens after testing

Fatigue cracks initiated from a corner of the notch for all fatigue specimens, as shown in Fig. 7. It can be seen that all the cracks could be distinguished visually as an optical bright area in the shape of ellipse quarter. On the fracture plane, the cracks initiated from the specimen surface, and propagated along a direction perpendicular to the specimen surface. It can be seen from the fracture plane that the cracks after LSP were visibly larger than those without LSP, and this is closely related to impacted crack propagation behavior of the alloy after LSP. LSP induces severe plastic deformation in the material, and the dislocation density in the alloy can be significantly increased [33]. The extremely deformed microstructure leads to impeded fatigue crack propagation behavior. Tan et al. studied the effect of LSP on the fatigue crack growth of a 2024-T3 aluminium alloy and reported that LSP is effective in suppressing the fatigue crack growth [34]. Zhang et al. found that the fatigue crack growth rates at a given stress intensity were reduced by over one order of magnitude [33]. Similar LSP-induced retardation effect of fatigue crack propagation has been widely reported [35-37]. The enlarged crack zone after LSP can be attributed to the retarded crack growth and the resulting longer crack growth path.

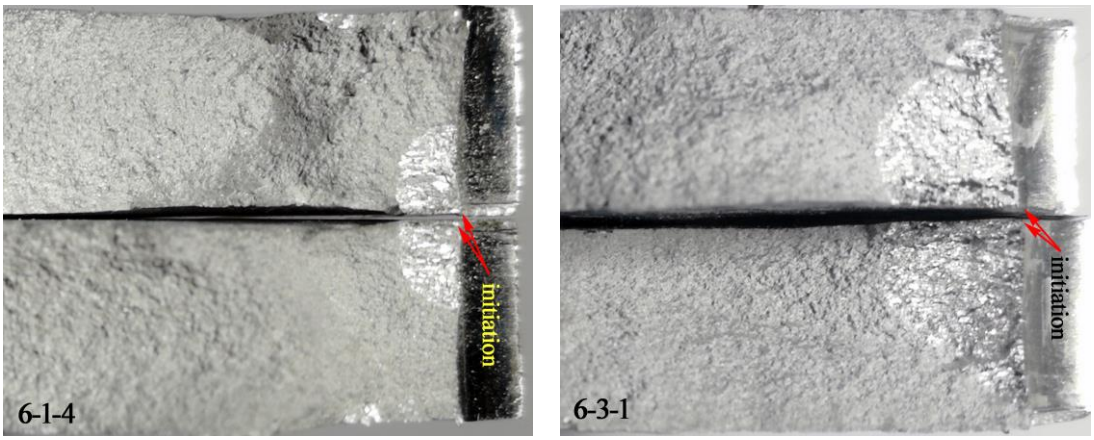

(a) 2024-T351 specimen without LSP (b) 2024-T351 specimen with LSP

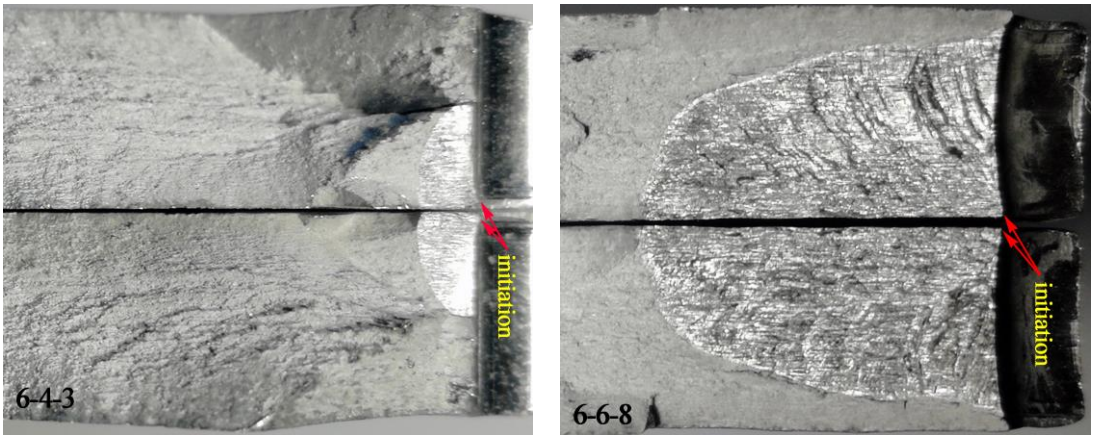

(c) 7050-T7451 specimen of raw material (d) 7050-T7451 specimen after LSP

Fig.7. Typical fractographies of the fatigue specimens

3. The TCD approach

3.1 The TCD

The TCD [25-27] has long been adopted in the field of fatigue life analysis, which is briefly expressed in Fig. 8

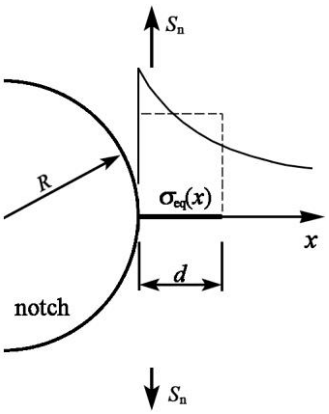

Fig.8. TCD approach

where S_n is nominal stress, $\sigma_{eq}(x)$ is equivalent stress on the fracture surface, d is critical distance and can be determined by the EI Haddad formula [38]

$$d = \frac{1}{\pi}\left(\frac{\Delta K_{th}}{\Delta \sigma_e}\right) \tag{1}$$

where $\Delta\sigma_e$ is fatigue limit, and ΔK_{th} .is the threshold value of stress intensity factor for fatigue crack propagation.

The equivalent stress $\sigma_{eq}(x)$ is dependent on the fatigue failure criterion and nominal stress S_n, so the equivalent stress at critical distance d can be written as

$$\sigma_{eq}(d) = \sigma_{eq}(x)\big|_{x=d} \tag{2}$$

3.2 Stress distribution in the double-edge-notched specimens

Numerical simulation was carried out to analyze the stress distribution of the specimen shown in Fig. 9. To simplify due to the specimen symmetry, a quarter of the specimen was taken as the object to be analyzed, as shown in Fig. 9(a). The virtual specimen was meshed using 1400 quadrangular elements, and the elements have been refined near the notch root with a minimum size of 0.005mm, as shown in Fig. 9(b).

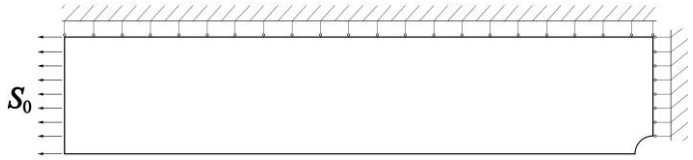

(a) Analysis model

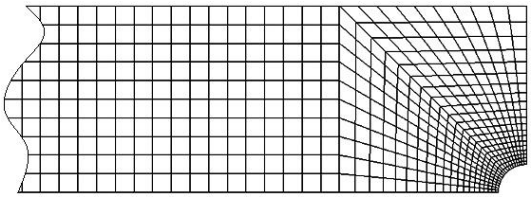

(b) FEA mesh

Fig. 9. FEM model

The Ramberg-Osgood model was used to express the cyclic constitutive equation of the two materials being investigated, see Eq. (3). The stress distribution at the narrowest section of the specimen is shown in Fig. 10. It can be seen from Fig.10 that the changing trend for the two materials

are identical. Under different fatigue loading, the location right at the notch root bears the maximum tensile stress, and the stress gradually decreases when the location is farther from the notch.

$$\varepsilon = \frac{\sigma}{E} + \left(\frac{\sigma}{K'}\right)^{\frac{1}{n'}} \tag{3}$$

According to the data from reference [28], in Eq. (3), the cyclic strength coefficient K' was taken equal to 655MPa and 743MPa respectively for 2024-T351 and 7050-T7451; the cyclic exponent n' to 0.065 and 0.089 respectively for 2024-T351 and 7050-T7451.

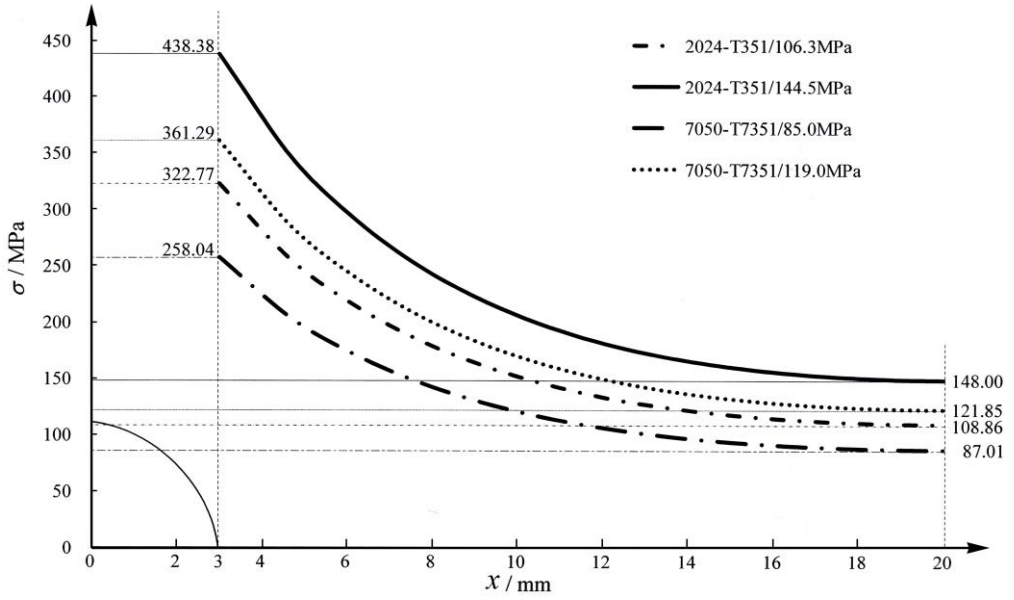

Fig. 10. Stress distribution at the narrowest section of the specimen

It can be seen that the theoretical stress concentration factor K_T of the specimen is 3.57, and the specimens are overall in elastic state.

3.3 Fatigue life prediction

Under the applied loading, the stress distribution near the notch can be obtained from Fig. 10 and Fig. 5b. LSP leads to the decrease of the maximum stress at the notch, however the stress gradient is large, see Fig. 11.

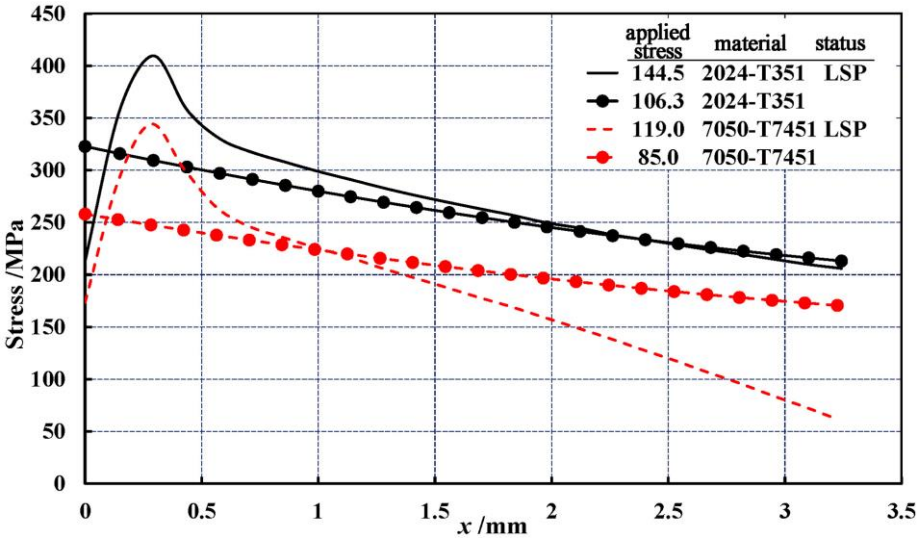

Fig.11. Resultant stress distribution under the applied load

According to the TCD, the fatigue life is controlled by the stress at the critical distance *d*. Based on the data listed in Table 3, the distance *d* can be calculated. The critical distance *d* is 0.144mm for 2024-T351 and 0.112mm for 7050-T7451, and then the $\sigma_{eq}(d)$ can be obtained by Fig. 11, see Table 5.

Table 5

Equivalent stress.

Material	2024-T351		7051-T7451	
	Without LSP	With LSP	Without LSP	With LSP
Applied stress /MPa	106.3	144.5	85.0	119.0
$\sigma_{eq}(d)$ /MPa	316.11	302.80	274.71	270.52

The S-N curves of aluminum alloy 2024-T351 and 7050-T7451 can be obtained from Ref. [31]. The S-N curves at stress ratio *R*=0.06 within 5×10^4~10^7 cycles are shown as follows

$$\begin{aligned} &\text{2024-T351} \quad \lg N_f = 27.8210 - 9.0779\lg(S_{max} + 29.3557) \\ &\text{7050-T7451} \quad \lg N_f = 103.409 - 32.1381\lg(S_{max} + 860.405) \end{aligned} \tag{4}$$

By substituting $\sigma_{eq}(d)$ into Eq. (4), the fatigue life N_f can be calculated and the results are

listed in Table 6. It can be seen that the predicted fatigue life is in good agreement with the experimental fatigue life, with the estimates being slightly conservative.

Table 6

Tested and predicted fatigue lives.

Material	2024-T351		7050-T7451	
	Without LSP	With LSP	Without LSP	With LSP
Logarithmic fatigue test life /cycles	5.1895	5.3748	5.3711	5.4260
Logarithmic predicted life /cycles	4.7776	4.9325	5.2261	5.2781
Logarithmic relative error	7.937%	8.229%	2.700%	2.728%

The predicted lives are obtained when the fatigue failure of the specimens occurs with the critical distance equaling to 0.144 mm or 0.112 mm, while the experimental fatigue lives are defined and obtained as the cycles to crack length of 1 mm. In fact, it is a more reasonable way to define the tested fatigue life as the cycles corresponding to a shorter crack, such as 0.1mm. However, due to the infeasibility of visually identifying a fatigue crack less than 1mm, the fatigue crack size was not adopted as a smaller value.

4 Conclusion

In this paper the effect of laser shock peening on the fatigue life of notched metallic specimens was studied experimentally and analytically. The LSP process was applied to notched specimens of two aluminum alloys. The residual stress around the notch was both measured by X-ray diffractometer, and simulated through numerical methods. The tensile and fatigue tests of the two

materials were carried out. The TCD was adopted in the prediction of the fatigue lifetime. The main conclusions are as summarized in what follows.

(1) Notches are fatigue critical parts where stress concentration can cause a decrease of fatigue life. The processing of laser shock peening is effective in enhancing the fatigue property of notched specimens by inducing compressive stress around the notch.

(2) The processing of laser shock peening can cause a more complex stress distribution at the notch. Along the direction of applied loading from the surface, the compressive stress increases first and then decreases until being replaced by tensile stress. The highest compressive stress lies in the layer near but a little below the surface.

(3) The process of laser shock peening is an effective method to improve the fatigue life of notched metallic components in engineering, and the life prediction of such components is particularly important for their application. This paper provides a practical way to predict the fatigue life of these specimens by introducing the effective stress after LSP into the theory of critical distance. The predicted fatigue lifetime is in sound agreement with the experimental results, which verifies the effectiveness of the proposed method in this paper.

Declaration of Competing Interest

The authors declare that they have no known competing financial interests or personal relationships that could have appeared to influence the work reported in this paper.

Acknowledgement

The authors gratefully acknowledge the financial support of the National Natural Science Foundation of China (52075244).

References

[1] Mironov S, Ozerov M, Kalinenko A, Stepanov N, Plekhov O, Sikhamov R, et al. On the relationship between microstructure and residual stress in laser-shock-peened Ti-6Al-4V. J Alloy Comp 2022;900:163383. https://doi.org/10.1016/j.jallcom.2021.163383

[2] Jiang YF, Ji B, Gan XD, Hua C, Li X, and Zhu H. Study on the effect of laser peening with different power densities on fatigue life of fastener hole. Opt Laser Technol 2018;106:311-20. https://doi.org/10.1016/j.optlastec.2018.04.025

[3] Spadaro L, Gomez-Rosas G, Rubio-González C, Bolmaro R, Chavez-Chavez A, and Hereñú S. Fatigue behavior of superferritic stainless steel laser shock treated without protective coating. Opt Laser Technol 2017;93:208-15. https://doi.org/10.1016/j.optlastec.2017.03.003

[4] Yella P, Rajulapati KV, Prasad Reddy GV, Sandhya R, Prem Kiran P, Buddu RK, et al. Effect of laser shock peening on high cycle fatigue characteristics of 316LN stainless steel. International Int J Pres Ves Pip 2019;176:103972. https://doi.org/10.1016/j.ijpvp.2019.103972

[5] Prabhakaran S, Kalainathan S, Shukla P, and Vasudevan VK. Residual stress, phase, microstructure and mechanical property studies of ultrafine bainitic steel through laser shock peening. Opt Laser Technol 2019;115:447-58. https://doi.org/10.1016/j.optlastec.2019.02.041

[6] Zhang Y, Zhang K, Hu Z, Chen T, Susmel L, and Wei B. The synergetic effects of shot peening and laser-shot peening on the microstructural evolution and fatigue performance of a medium carbon steel. Int J Fatigue 2023;166:107246. https://doi.org/10.1016/j.ijfatigue.2022.107246

[7] Dwivedi PK, Vinjamuri R, Rai AK, Ganesh P, Ranganathan K, Bindra KS, et al. Effect of laser shock peening on ratcheting strain accumulation, fatigue life and bulk texture evolution in HSLA steel. Int J Fatigue 2022;163:107033. https://doi.org/10.1016/j.ijfatigue.2022.107033

[8] Azevedo L, Kashaev N, Horstmann C, Ventzke V, Furtado C, Moreira PMGP, et al. Fatigue behaviour of laser shock peened AISI D2 tool steel. Int J Fatigue 2022;165:107226. https://doi.org/10.1016/j.ijfatigue.2022.107226

[9] Lu JZ, Luo KY, Dai FZ, Zhong JW, Xu LZ, Yang CJ, et al. Effects of multiple laser shock processing (LSP) impacts on mechanical properties and wear behaviors of AISI 8620 steel. Mat Sci Eng A 2012;536:57-63. https://doi.org/10.1016/j.msea.2011.12.053

[10] Bikdeloo R, Farrahi GH, Mehmanparast A, and Mahdavi SM. Multiple laser shock peening effects on residual stress distribution and fatigue crack growth behaviour of 316L stainless steel. Theor Appl Fract Mec 2020;105:102429. https://doi.org/10.1016/j.tafmec.2019.102429

[11] Li W, Chen H, Huang W, Chen J, An S, Xiao G, et al. Optimization of multiple laser shock peening on high-cycle fatigue performance of aluminized AISI 321 stainless steel. Int J Fatigue 2021;153:106505. https://doi.org/10.1016/j.ijfatigue.2021.106505

[12] Correa C, Ruiz de Lara L, Díaz M, Gil-Santos A, Porro JA, and Ocaña JL. Effect of advancing direction on fatigue life of 316L stainless steel specimens treated by double-sided laser shock peening. Int J Fatigue 2015;79:1-9.
https://doi.org/10.1016/j.ijfatigue.2015.04.018

[13] Adu-Gyamfi S, Ren XD, Larson EA, Ren Y, and Tong Z. The effects of laser shock peening scanning patterns on residual stress distribution and fatigue life of AA2024 aluminium alloy. Opt Laser Technol 2018;108:177-85.
https://doi.org/10.1016/j.optlastec.2018.06.036

[14] Larson EA, Ren X, Adu-Gyamfi S, Zhang H, and Ren Y. Effects of scanning path gradient on the residual stress distribution and fatigue life of AA2024-T351 aluminium alloy induced by LSP. Results Phys 2019;13:102123.
https://doi.org/10.1016/j.rinp.2019.02.059

[15] van Aswegen DC, and Polese C. Experimental and analytical investigation of the effects of laser shock peening processing strategy on fatigue crack growth in thin 2024 aluminium alloy panels. Int J Fatigue 2021;142:105969.
https://doi.org/10.1016/j.ijfatigue.2020.105969

[16] Luo KY, Lu JZ, Wang QW, Luo M, Qi H, and Zhou JZ. Residual stress distribution of Ti-6Al-4V alloy under different ns-LSP processing parameters. Appl Surf Sci 2013;285:607-15.
https://doi.org/10.1016/j.apsusc.2013.08.100

[17] Wei XL, and Ling X. Numerical modeling of residual stress induced by laser shock processing. Appl Surf Sci 2014;301:557-63.
https://doi.org/10.1016/j.apsusc.2014.02.128

[18] Salimianrizi A, Foroozmehr E, Badrossamay M, and Farrokhpour H. Effect of Laser Shock Peening on surface properties and residual stress of Al6061-T6. Opt Laser Eng 2016;77:112-7.
https://doi.org/10.1016/j.optlaseng.2015.08.001

[19] Keller S, Chupakhin S, Staron P, Maawad E, Kashaev N, and Klusemann B. Experimental and numerical investigation of residual stresses in laser shock peened AA2198. J Mater Process Tech 2018;255:294-307.
https://doi.org/10.1016/j.jmatprotec.2017.11.023

[20] Gao Y, Yang W, Huang Z, and Lu Z. Effects of residual stress and surface roughness on the fatigue life of nickel aluminium bronze alloy under laser shock peening. Eng Fract Mech 2021;244:107524.
https://doi.org/10.1016/j.engfracmech.2021.107524

[21] Sanchez AG, You C, Leering M, Glaser D, Furfari D, Fitzpatrick ME, et al. Effects of laser shock peening on the mechanisms of fatigue short crack initiation and propagation of AA7075-T651. Int J Fatigue 2021;143:106025.
https://doi.org/10.1016/j.ijfatigue.2020.106025

[22] Cuellar SD, Hill MR, DeWald AT, and Rankin JE. Residual stress and fatigue life in laser shock peened open hole samples. Int J Fatigue 2012;44:8-13.
https://doi.org/10.1016/j.ijfatigue.2012.06.011

[23] Ivetic G, Meneghin I, Troiani E, Molinari G, Ocaña J, Morales M, et al. Fatigue in laser shock peened open-hole thin aluminium specimens. Mate Sci Eng A 2012;534:573-9.
https://doi.org/10.1016/j.msea.2011.12.010

[24] Sun R, Che Z, Cao Z, Zhang H, Zou S, Wu J, et al. Effect of laser shock peening on high cycle

fatigue failure of bolt connected AA2024-T351 hole structures. Eng Fail Anal 2022;141:106625. https://doi.org/10.1016/j.engfailanal.2022.106625

[25] Taylor D. Analysis of fatigue failures in components using the theory of critical distances. Eng Fail Anal 2005;12(6):906-14. https://doi.org/10.1016/j.engfailanal.2004.12.007

[26] Susmel L, and Taylor D. A simplified approach to apply the theory of critical distances to notched components under torsional fatigue loading. Int J Fatigue 2006;28(4):417-30. https://doi.org/10.1016/j.ijfatigue.2005.07.035

[27] Susmel L. The theory of critical distances: a review of its applications in fatigue. Eng Fract Mech 2008;75(7):1706-24. https://doi.org/10.1016/j.engfracmech.2006.12.004

[28] Yao WX. Stress field intensity approach for predicting fatigue life. Int J Fatigue 1993;15(3):243-6. https://doi.org/10.1016/0142-1123(93)90182-P

[29] Susmel L, Tovo R, and Benasciutti D. A novel engineering method based on the critical plane concept to estimate the lifetime of weldments subjected to variable amplitude multiaxial fatigue loading. Fatigue Fract Eng M 2009;32(5):441-59. https://doi.org/10.1111/j.1460-2695.2009.01349.x

[30] Shang D-G, Wang D-K, Li M, and Yao W-X. Local stress–strain field intensity approach to fatigue life prediction under random cyclic loading. Int J Fatigue 2001;23(10):903-10. https://doi.org/10.1016/S0142-1123(01)00051-2

[31] Wu X. Handbook of Mechanical Properties of Aircraft Structural Metals. Beijing: Aviation Industry Press; 1996.

[32] Duggan TV, and Byrne J. In: Duggan TV, and Byrne J eds. Fatigue as a Design Criterion. London: Macmillan Education UK; 1977:94-111.

[33] Zhang，Hong, and Yu C. Laser shock processing of 2024-T62 aluminum alloy. Mat Sci Eng A 1998;257(2):322-7. https://doi.org/10.1016/S0921-5093(98)00793-X

[34] Tan Y, Wu G, Yang JM, and Pan T. Laser shock peening on fatigue crack growth behaviour of aluminium alloy. Fatigue Fract Eng M 2004;27(8):649-56. https://doi.org/10.1111/j.1460-2695.2004.00763.x

[35] Zhao J, Dong Y, and Ye C. Laser shock peening induced residual stresses and the effect on crack propagation behavior. Int J Fatigue 2017;100:407-17. https://doi.org/10.1016/j.ijfatigue.2017.04.002

[36] Ge M-Z, and Xiang J-Y. Effect of laser shock peening on microstructure and fatigue crack growth rate of AZ31B magnesium alloy. J Alloy Compd 2016;680:544-52. https://doi.org/10.1016/j.jallcom.2016.04.179

[37] Sun R, Li L, Guo W, Peng P, Zhai T, Che Z, et al. Laser shock peening induced fatigue crack retardation in Ti-17 titanium alloy. Mater Sci Eng A 2018;737:94-104. https://doi.org/10.1016/j.msea.2018.09.016

[38] El Haddad MH, Topper TH, and Smith KN. Prediction of non propagating cracks. Eng Fract Mech 1979;11(3):573-84. https://doi.org/10.1016/0013-7944(79)90081-X (1979).